RSC Sustainability

ROYAL SOCIETY OF CHEMISTRY

PAPER

View Article Online
View Journal | View Issue



Cite this: *RSC Sustainability*, 2023, **1**, 2319

# N-doped graphene nanosheets-based optical nano switch for the selective detection of guanine and $Pb^{2+}$

Vijayendra Kumar Tripathi,†[ab] Gouri Sankar Das,†[c] Raju Kumar Gupta,[adef] Manish Srivastava *[g] and Kumud Malika Tripathi *[c]

The development of biosensors for the selective detection of $Pb^{2+}$ and guanine is critical for the elucidation of lead toxicity and human health monitoring. In this research, blue-green luminous water-soluble nitrogen-doped graphene nanosheets (ws-NGNSs) were synthesized from biomass as an optical sensor for guanine and $Pb^{2+}$ in aqueous media. A facile hydrothermal approach followed by mild oxidation was used for the synthesis of ws-NGNSs, where rotten pear was used as the carbon source and urea was used as the nitrogen source. The ws-NGNSs emitted intense fluorescence at a maximum excitation/emission wavelength of 340/425 nm. The addition of $Pb^{2+}$ effectively quenched the blue-green emission of ws-NGNSs with prominent selectivity. The selectivity is attributed to the synergic effects of heteroatom doping, surface functional groups, and surface-active sites. Further, ws-NGNSs/$Pb^{2+}$ was used as a promising fluorescent probe for the selective recognition of guanine. The addition of guanine induced the fluorescence "turn on" effect. Therefore, ws-NGNSs with excellent fluorescence properties can be used as efficient fluorescence "on-off-on" nano-switches for the selective detection and differentiation of $Pb^{2+}$ and guanine with limits of detection of 8 μM and 0.2 μM, respectively. The possible sensing mechanism is explained using fluorescence and UV-vis spectroscopy. Water-soluble NGNSs have a solid foundation for the fabrication of optical sensors for biomedical and environmental applications.

Received 17th September 2023
Accepted 16th October 2023

DOI: 10.1039/d3su00328k

rsc.li/rscsus



### Sustainability spotlight

Heteroatom-doped nanocarbons are more promising environment-friendly and cost-effective fluorescent materials than traditional metal-based quantum dots for biomedical/environmental applications. However, the synthesis of heteroatom-doped nanocarbons *via* energy-intensive processes, the use of hazardous chemicals and extremely clean gases are further causing environmental concerns, which necessitate a transition to a green and energy-efficient synthesis process, where biomass can be used as a carbon source. The detection, differentiation, and monitoring of $Pb^{2+}$ concentration in drinking water are highly required for the better monitoring of water quality and human health maintenance. To realize this goal, we synthesized N-doped water-soluble graphene nanosheets (ws-NGNSs) by a straightforward, economical, and environment-friendly approach through the hydrothermal carbonization of a pear-urea mixture as a carbon-nitrogen source. The exploration of ws-NGNSs as an optical nano-switch for environmental and biomedical applications for the selective detection and discrimination of $Pb^{2+}$ and guanine was also explored. This work is consistent with the WHO's and UN's sustainable development goals of clean water and sanitation (SDG 6), good health/well-being (SDG 3), responsible production (SDG 12), and sustainable industrialization (SDG 9).

## 1. Introduction

While the technological advancements and enhancements in lifestyle offer humans an easy life, they have brought critical environmental concerns and after-effects.[1] The threats from water pollution constitute a huge human healthcare challenge and an enormous medical and financial burden around the world.[2] The contamination of natural water reservoirs by heavy metal ions from the earth's crust and anthropogenic activities, such as from domestic, agricultural, and industrial effluents, affect the balance of the aquatic ecosystem and human health.[3] The release of wastewater contaminated with heavy metal ions poses serious environmental challenges.[1] Heavy metal ions

[a]*Department of Chemical Engineering, Indian Institute of Technology, Kanpur, 208016, India*
[b]*Department of Chemistry, Banasthali Vidyapith, Newai, Rajasthan 304022, India*
[c]*Department of Chemistry, Indian Institute of Petroleum and Energy, Visakhapatnam, Andhra Pradesh, 530003, India. E-mail: kumud@iipe.ac.in; kumud20010@gmail.com*
[d]*Department of Sustainable Energy Engineering, Indian Institute of Technology Kanpur, Kanpur, 208016, UP, India*
[e]*Center for Environmental Science and Engineering, Indian Institute of Technology Kanpur, Kanpur, 208016, UP, India*
[f]*Chandrakanta Kesavan Centre for Energy Policy and Climate Solutions, Indian Institute of Technology Kanpur, Kanpur, 208016, UP, India*
[g]*Department of Chemistry, Allahabad University, Allahabad, India. E-mail: sagermanish1@gmail.com*
† Equal contribution.

negatively impact living organisms because of their high water solubility and toxicity, low biodegradability, carcinogenic nature, and environmental persistence.[4–6] Therefore, the efficient removal of heavy metal ions is the foremost crucial step for meeting the needs of a sustainable society and environment. Lead (Pb), with unquestionable toxicity, has been released into natural water from electroplating, paints, anti-corrosive coatings, mining, battery recycling, chemicals, alloys, textiles, and other industries and consumer products.[7] $Pb^{2+}$ has a relatively long biological half-life with high bioaccumulation capacity.[8] Ingestion of lead even at low concentration can have various harmful impacts on human health, such as dysfunction of the nervous system, renal failure, gastrointestinal diseases, anemia, DNA damage, genotoxicity, coronary disease, mental-health issues, and growth retardation.[9,10] Therefore the detection, differentiation, and monitoring of $Pb^{2+}$ concentrations in drinking water are highly required.[8] Various analytical techniques, such as atomic absorption spectrophotometry, electrochemistry protocols, and inductively coupled plasma-atomic emission spectrometry are effective for the quantification of $Pb^{2+}$.[11] However, they are not suitable for on-site analyses and hands-on applications and demand tedious operational and sample preparation processes.

Guanine (G) is an essential nitrogenous base component of deoxyribonucleic acid (DNA) ribonucleic acid (RNA) and is also one of the final metabolic products of nucleic acid oxidation.[12] Guanine plays a crucial role in the transformation/storage of genetic information and protein biosynthesis.[13] Guanine has been proposed as a biomarker for the observation of essential cellular activities such as energy transduction, enzyme formation and signal transduction. Studies have shown that guanine can be oxidized by various oxidants and free radicals.[14,15] The abnormal concentration of guanine and its derivatives can play a crucial role in monitoring human health for the diagnosis of diseases such as cancer, immunodeficiency syndrome (AIDS), epilepsy and human immunodeficiency virus (HIV) infection.[15] Therefore, the detection, identification, discrimination and quantification of guanine and its derivatives in extracellular/intracellular environments is of great significance in bioscience and clinical diagnosis.[12] Currently, various analytical methods such as high-performance liquid chromatography,[16] fluorescence,[17,18] electrochemical,[19,20] and capillary electrophoresis (CE)[21] have been utilized for the recognition of guanine. The selectivity and sensitivity of the above processes are dominated by the use of artificial receptors, where the presence of an organic co-solvent is vital for the operation and it generally exhibits a low affinity for guanine.[22] In this context, the optical technique has been proven more effective because of promising advantages such as convenient visual detection, applicability in both solution and solid phases, operational simplicity and unique selectivity.

Simple, eco-friendly, fast responsive, very sensitive, and selective fluorescence sensors based on nanomaterials are gaining popularity among the various analytical techniques. The development of fluorescence sensors in the ultrasensitive and accurate detection of heavy metal ions/biomolecules has been required to investigate human health issues.[23] The 2D and 3D-graphene-based nanomaterials have been at the forefront of chemical and biological sensors in recent years. Graphene-based fluorescent sensors have been realized as quick and effective multi-responsive optical probes for the detection of various substances.[24–26] The unique characteristics of graphene-based nanomaterials including high specific surface area, high quenching ability, extraordinary electron transport capabilities, high chemical stability, edges, defects and quantum confinement effects make them suitable for utilization in various optoelectronic applications.[27] Heteroatom doping in graphene-based materials also changes the microstructure of the hexagonal carbon skeleton and causes a redistribution of charges, which can induce fascinating optical properties and enhanced catalytic centers.[28] N is the obvious choice for the doping of graphene because of its size and compatible electronegativity with carbon atoms.[28,29] However, the conventional techniques for the synthesis of nitrogen-doped graphene nanosheets (N-GNSs) demand complex and time-consuming protocols and expensive precursors. In addition, the use of hazardous chemicals, expensive equipment, and extremely clean gas is causing further environmental concerns.[30] From this viewpoint, naturally available precursors such as lentils,[26] dead leaves,[31] cellulose,[32] silkworm powder[33] and chitosan[34] with nominal processing are at the forefront for the synthesis of heteroatom-doped carbon nanostructures.[35,36]

Herein, we report the synthesis of water-soluble nitrogen-doped graphene nanosheets (ws-NGNSs) as a fluorescence nano-switch sensor for heavy metal ion/biomolecule detection. The ws-NGNSs were green-synthesized from a mixture of pear fruit as a carbon source and urea as a nitrogen source by hydrothermal carbonization followed by mild acid oxidation. The as-synthesized ws-NGNSs showed good aqueous solubility and tunable emissions throughout the visible range. Water-soluble NGNSs provide a means for the selectivity and discrimination of other metal/bimolecular species. More significantly, the sensitivity was achieved without the addition of any surface passivating agent or composite fabrication. Therefore, ws-NGNSs can be used as an optical nano switch for water remediation and the monitoring of human health issues.

## 2. Results and discussion

The ws-NGNSs were synthesized using a straightforward, economical and environmentally friendly approach through the hydrothermal carbonization of a pear-urea mixture as carbon and nitrogen sources at 220 °C for 48 h, followed by mild acid oxidation. Fig. 1 presents a schematic representation of the ws-NGNSs synthesis process. During hydrothermal carbonization, the urea and pear were thermo-chemically converted into carbon nanostructures *via* a series of reactions including hydrolysis, dehydration, polymerization intramolecular dehydration and carbonization *via* condensation and aromatization reactions, with the subsequent carbonization of pear using subcritical water through fractionation.[37,38] Urea plays a critical role in hydrothermal carbonization by introducing N doping in graphene nanosheets *via* the formation of $NH_3$.[39] However, the appropriate mechanism still needs to be explored. Mild acid

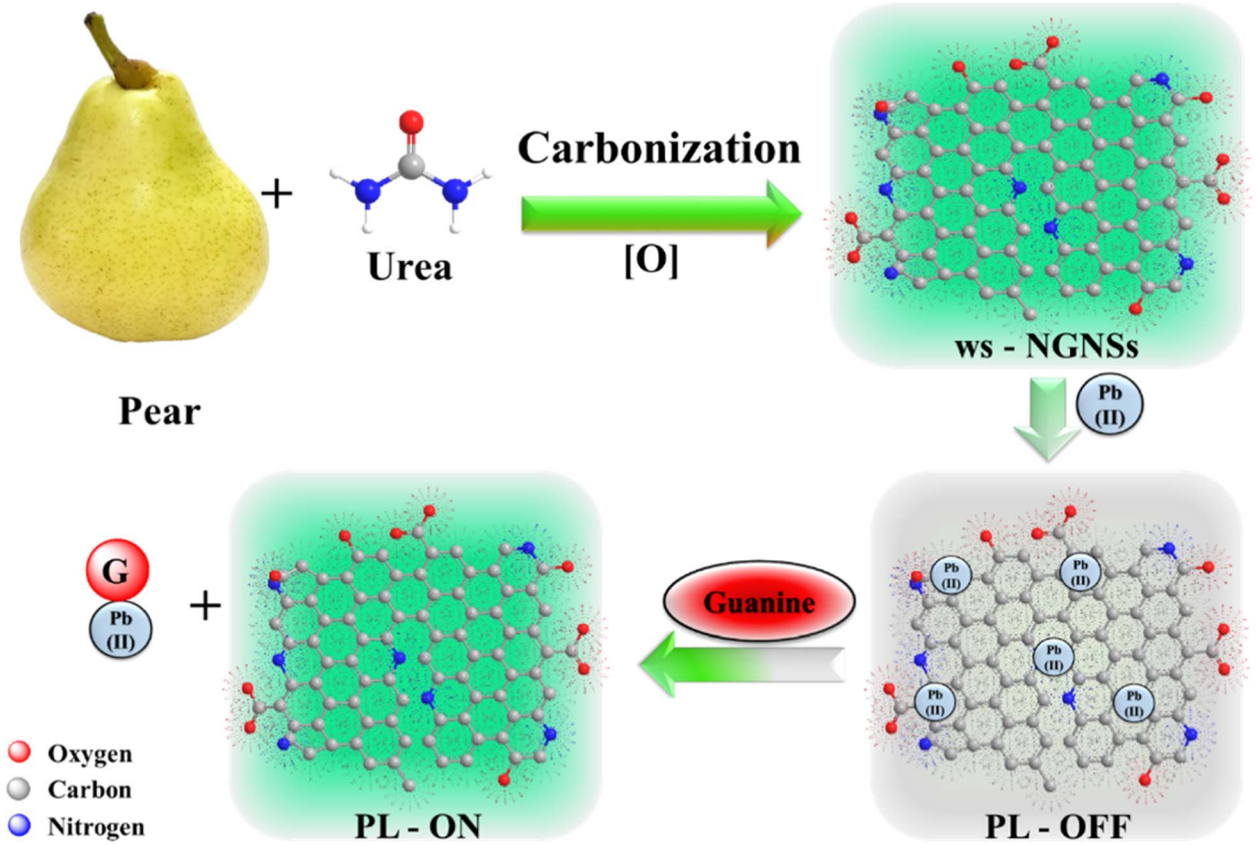


Fig. 1 Schematic representation of the synthesis procedure of ws-NGNSs from biomass and its working principle as an "on-off-on" fluorescence probe for the rapid detection and discrimination of $Pb^{2+}$ and guanine.

treatment was carried out to get water solubility in N-GNSs. The as-synthesized ws-NGNSs emitted throughout the blue-green region as a function of excitation wavelength. The exploration of ws-NGNSs as an optical nano-switch for environmental and biomedical applications for the selective detection and discrimination of $Pb^{2+}$ and guanine is also shown in Fig. 1.

### 2.1 Optical properties

The optical characteristics of the as-synthesized ws-NGNSs were investigated with UV-vis and fluorescence spectral analysis. The UV-vis absorption spectrum of the aqueous solution of ws-NGNSs in Fig. 2a shows an absorption peak centered at 278 nm owing to the $\pi$–$\pi^*$ transition of the aromatic $sp^2$ domains and the n–$\pi^*$ electronic transition between lone pairs of N/O and $sp^2$ carbon atoms in the graphitic framework.[40] The aqueous solution of ws-NGNSs shows a light yellow color in the ambient daylight but turns to bright blue when exposed to 365 nm UV light, as shown in the insets of Fig. 2a. Fig. 2b displays the excitation-dependent PL emission spectra of ws-NGNSs ranging from 300 to 520 nm, which showed a red shift in emission and a decrease in emission intensity when the excitation wavelength changed from 360 nm to 520 nm. It is evident that ws-NGNSs generate a high-intensity bright blue-green emission at an optimum excitation wavelength of 340 nm. The hydrophilic surface functional groups of ws-NGNSs provide high aqueous solubility and intense fluorescence. These properties are the backbone for the selective sensing of heavy metal ions and biomolecules.[41,42]

### 2.2 Morphological and structural properties of ws-NGNSs

The surface morphology and microstructure of ws-NGNSs were characterized using SEM, TEM, and high-resolution TEM (HRTEM) microscopic measurements. The SEM images in Fig. 3a and b show the formation of nanosheets and the absence of any other morphological impurities. The low-resolution TEM image in Fig. 3c and d shows a typical highly crumpled nanosheet structure of ws-NGNSs with an entangled character. These structural characteristics were attributed to an increase in surface area and the density of active sites in ws-NGNSs.[43] The HRTEM image of ws-NGNSs in Fig. 3e indicated a uniform graphitic network with a high density of surface defects and an interplanar lattice distance of 0.29 nm.[44] The HRTEM image also revealed that ws-NGNSs was composed of few layers of graphene as indicated by the white circle.

The FTIR spectrum of ws-NGNSs in Fig. 3f supports the presence of oxygenated functional groups. The presence of an O–H and N–H functional group on the surface of ws-NGNSs is indicated by the broad peak at ~3500–3000 $cm^{-1}$.[45] The doublet at ~2974 $cm^{-1}$, ~2928 $cm^{-1}$, and a sharp peak at ~1033 $cm^{-1}$ are due to $sp^3$ C–H bond vibrations.[26] The band at ~1712 $cm^{-1}$

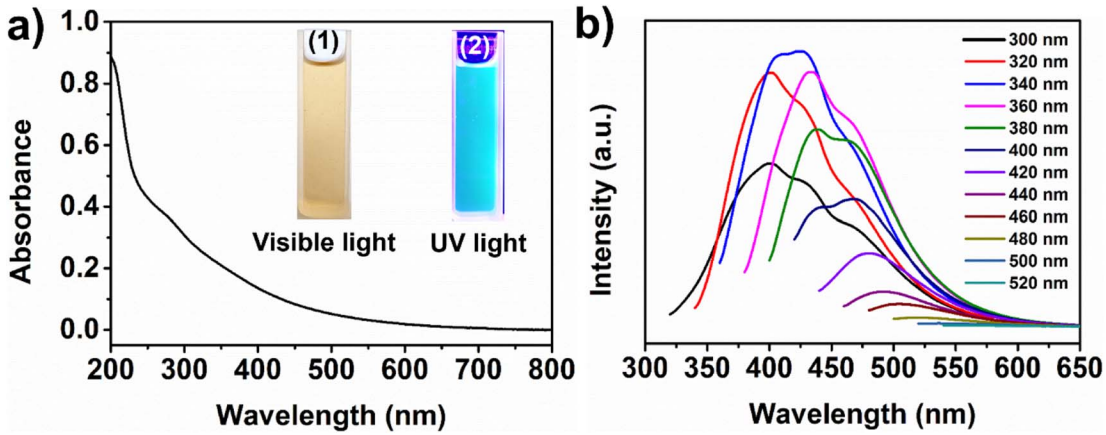


Fig. 2 Optical properties of ws-NGNSs. (a) Ultraviolet-visible absorption spectrum; inset: digital image of ws-NGNSs solution taken in visible light (1) and ultraviolet light (excitation, 365 nm) (2). (b) Fluorescence emission spectra at different excitation wavelengths.

is attributed to the vibrations of the C=O bond in the stretching mode.[46] The sharp peak at ~1629 $cm^{-1}$ is associated with the stretching vibrations of combined C=N and C=C bonds. The vibrations of C–N, C–O, and $sp^2$ C–H bonds were observed at ~1450 $cm^{-1}$, ~1201 $cm^{-1}$ and ~752 $cm^{-1}$, respectively.[26] The Raman spectrum of ws-NGNSs in Fig. 3g shows two distinct peaks at ~1348 $cm^{-1}$ (D band, defective mode) and ~1582 $cm^{-1}$ (vertical vibration mode, G band of graphitic structures).[47] The D band is attributed to the scattering of phonons at the edge of disordered graphene and the G band originated from the vibration of the $sp^2$ carbons of graphene layers under the $E_2g$ mode.[48,49] The robust and intense D bands of ws-NGNSs

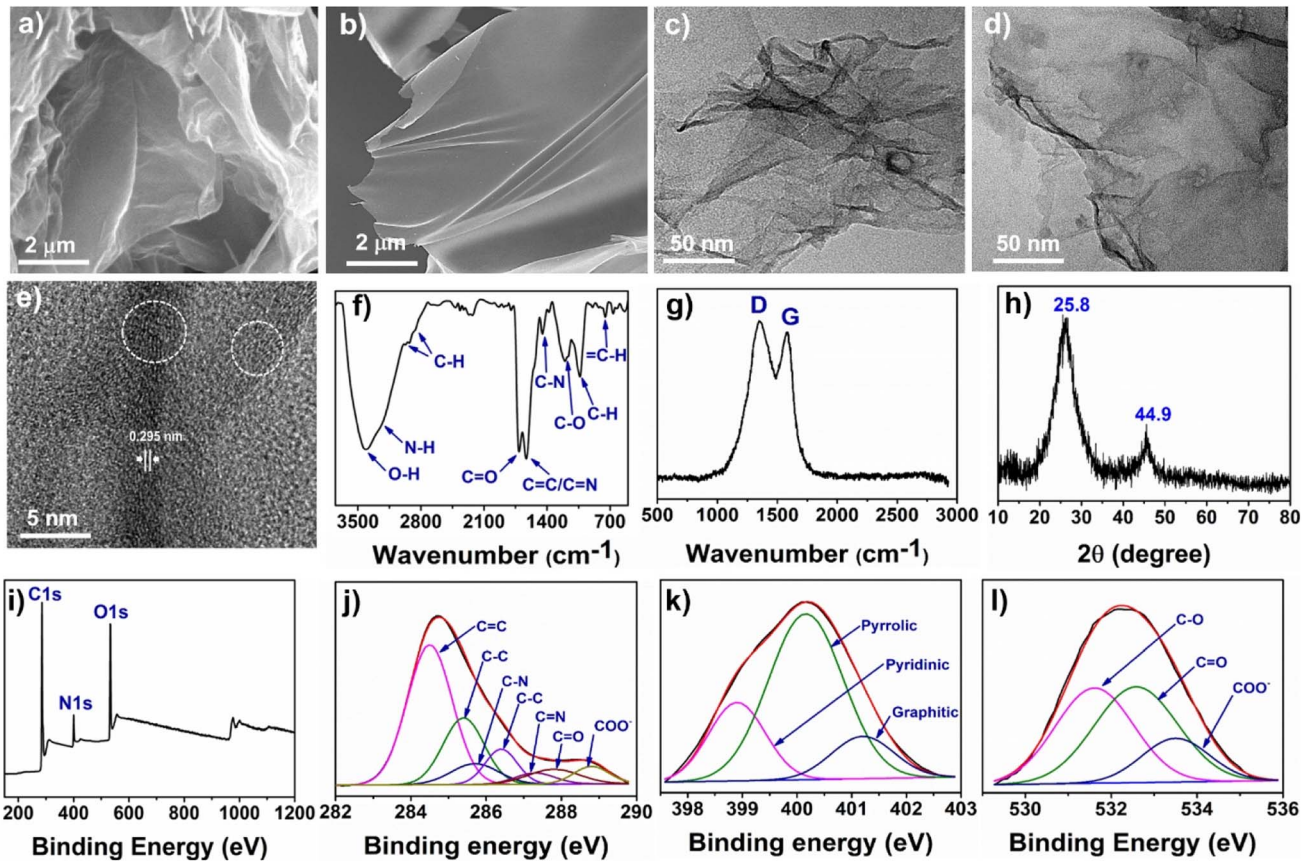


Fig. 3 The morphological and structural characterization of ws-NGNSs synthesized from pear. SEM images (a) and (b) showing the nanosheet-like structure; (c) and (d) TEM images; (e) HRTEM with interlayer space; (f) FTIR spectrum; (g) Raman spectrum; (h) XRD pattern; (i) XPS survey scan spectrum; high-resolution XPS spectra of C 1s (j), N 1s (k), and O 1s (l).

revealed disordered graphitic structures. The disorder density can be expressed as a ratio of the peak intensity of the D-band to the G-band, which is represented as $I_D/I_G$. The high degree of heteroatom doping enhanced the structural disorder of graphitic carbon and consequently, the high $I_D/I_G$ ratio. The high $I_D/I_G$ ratio of 1.75 indicates the presence of a high density of disorder in the aromatic $sp^2$-carbons of ws-NGNSs.[50]

The X-ray diffraction (XRD) analysis was implemented to detect the crystallinity of the as-synthesized ws-NGNSs. The XRD pattern in Fig. 3h shows a broad peak at $2\theta = 25.8°$ corresponding to the (002) face and a weak peak at $2\theta = 44.9°$ corresponding to the (101) face of graphitic carbon.[38] The lack of additional peaks suggests the high purity of synthesized materials. The surface chemical composition, $SP^3/SP^2$ bonding environment of carbon, heteroatom doping and N-configurations can be obtained by XPS analysis.[46,51] The XPS survey scan spectrum of the ws-NGNSs in Fig. 3i shows the presence of three prominent bands located at 385.1 eV, 400.1 eV and 532.1 eV, these bands confirmed the presence of C (67.2%), O (27.4), and N (5.4%), respectively. The high-resolution C1s spectra in Fig. 3j are de-convoluted into seven peaks at 284.4 eV, 285.4 eV, 285.8 eV, 286.4 eV, 287.3 eV, 287.6 eV and 288.9 eV, confirming the existence of C=C, C–C, C–N, C–N, C=N, C–O, C=O and $COO^-$ bonding of carbon, respectively.[52] The incorporation of nitrogen atoms into the carbon skeleton of ws-NGNSs was revealed by the presence of three bonding configurations of nitrogen. The pyridinic (peak at 398.95 eV), pyrrolic (peak at 400.11 eV), and graphitic (peak at 401.2 eV)[53] bonding configurations are identified in de-convoluted N 1s spectra as shown in Fig. 3k. The high-resolution O1s spectra of ws-NGNSs in Fig. 3l display the different bonding configurations of oxygen as C–O, C=O, and $COO^-$ centered at 531.62 eV, 532.58 eV and 533.6 eV, respectively.[53]

### 2.3 Detection of $Pb^{2+}$ and guanine

Fluorescence spectroscopy was used to investigate the sensing capability of ws-NGNSs for metal cations, anions, and neutral analytes. A 10 μL aqueous solution of different metal ions (1 mM) was added to the 2.5 mL aqueous solution of ws-NGNSs, and the fluorescence intensity of ws-NGNSs was recorded. The relative fluorescence intensity was unaffected by the addition of various metal ions except for $Pb^{2+}$ (Fig. 4a). The addition of $Pb^{2+}$ resulted in considerable quenching of the blue-green emission of ws-NGNSs, which indicated the high selectivity of ws-NGNSs towards $Pb^{2+}$ (Fig. 4b). The PL intensity of ws-NGNSs was quenched upon interaction with $Pb^{2+}$ ions due to the energy dissipation of excited states in a non-radiative electronic transition. A consistent decrease in the emission intensity of ws-NGNSs was observed with $Pb^{2+}$ addition till the maximum, and the quenching ratio $I/I_0$ (where $I_0$ is the emission of ws-NGNSs and $I$ is the emission of ws-NGNSs after the addition of $Pb^{2+}$) is shown by Stern–Volmer (S–V) plots in Fig. 4c. The extent of quenching intensity ($I/I_0$) is inversely proportional to the concentration of $Pb^{2+}$ as shown in Fig. 4c. The selectivity towards $Pb^{2+}$ as compared to other cations is attributed to the formation of a stable complex between the nitrogenous and oxygenated functional groups of ws-NGNSs and $Pb^{2+}$ *via* a complexation reaction.[54] These new complexes can effectively "turn-off" the fluorescence intensity with a limit of detection of 8 μM as calculated by the standard S–V plot.[55]

The PL responses of the ws-NGNSs/$Pb^{2+}$ system to different biomolecules, including adenine, guanine, thymine, cytosine, aspartic acid, ascorbic acid, urea and thiourea, were investigated. It was observed that only guanine could selectively "turn on" the quenched PL intensity of the ws-NGNSs/$Pb^{2+}$ system as shown in Fig. 4d. This revealed the excellent selectivity of the ws-NGNSs/$Pb^{2+}$ system for the discrimination of guanine. The high selectivity towards guanine was achieved because of the strong co-ordination of guanine to the ws-NGNSs/$Pb^{2+}$ system in contrast to ws-NGNSs. The PL emission of the ws-NGNSs/$Pb^{2+}$ system showed a linear increase in intensity when guanine concentration was increased from 0 μM to 25 μM (Fig. 4e). The limit of detection was calculated, following a standard 3d/m method, from the linear response of the S–V plot[56] in Fig. 4f to be 0.2 μM.

The ws-NGNSs selectively detected $Pb^{2+}$ *via* PL quenching and the quenched system of ws-NGNSs/$Pb^{2+}$ responded to guanine by the restoration of the quenched PL with the utmost selectivity. This property of ws-NGNSs was explored for its potential application as a "fluorescent-nano-switch" for the selective sensing of $Pb^{2+}$ and guanine for up to four cycles as shown in Fig. 5a and b. The ws-NGNSs act as an efficient "on–off–on" optical probe controlled by the $Pb^{2+}$ and guanine concentrations with excellent reversibility.

### 2.4 The plausible mechanism of fluorescence "on-off-on" mechanism

The plausible mechanism for the fluorescence "on-off-on" control by the $Pb^{2+}$ and guanine can be explained on the basis of fluorescence resonance energy transfer (FRET) and the photon-induced electron transfer (PET) processes.[57] These two phenomena are involved in the ws-NGNSs-based PL probe for the detection and discrimination of $Pb^{2+}$ and guanine. The FRET mechanism includes a process of non-radiative energy transfer between donor molecules and acceptor molecules. In contrast, the PET mechanism consists of a method of charge transfer between donor molecules and acceptor molecules. However, heavy metal ions ($Pb^{2+}$) have a strong tendency to form complexes with the heteroatom (nitrogen and oxygen)-containing functional groups of ws-NGNSs. The N-doping and oxygenous functional groups on the surface of ws-NGNSs played a crucial role in achieving the selective detection of $Pb^{2+}$. The availability of such functional groups allows metal ions to diffuse and adsorb on the surface of the ws-NGNSs in a selective manner.[58,59] As a result, fluorescence quenching occurs without any spectral shift, due to the reduction of the energy gap between the ws-NGNSs and $Pb^{2+}$ through charge transfer. The change in the local density of states was also evident for the same.[60,61]

A plausible mechanistic explanation for the fluorescence quenching through the ws-NGNSs/$Pb^{2+}$ system is demonstrated in Fig. 5a. The positively charged metal ions were attracted by the negatively charged functional groups of ws-NGNSs *via* electrostatic interaction, which reduced the distance between ws-NGNSs and $Pb^{2+}$ and strengthened the ws-NGNSs/$Pb^{2+}$

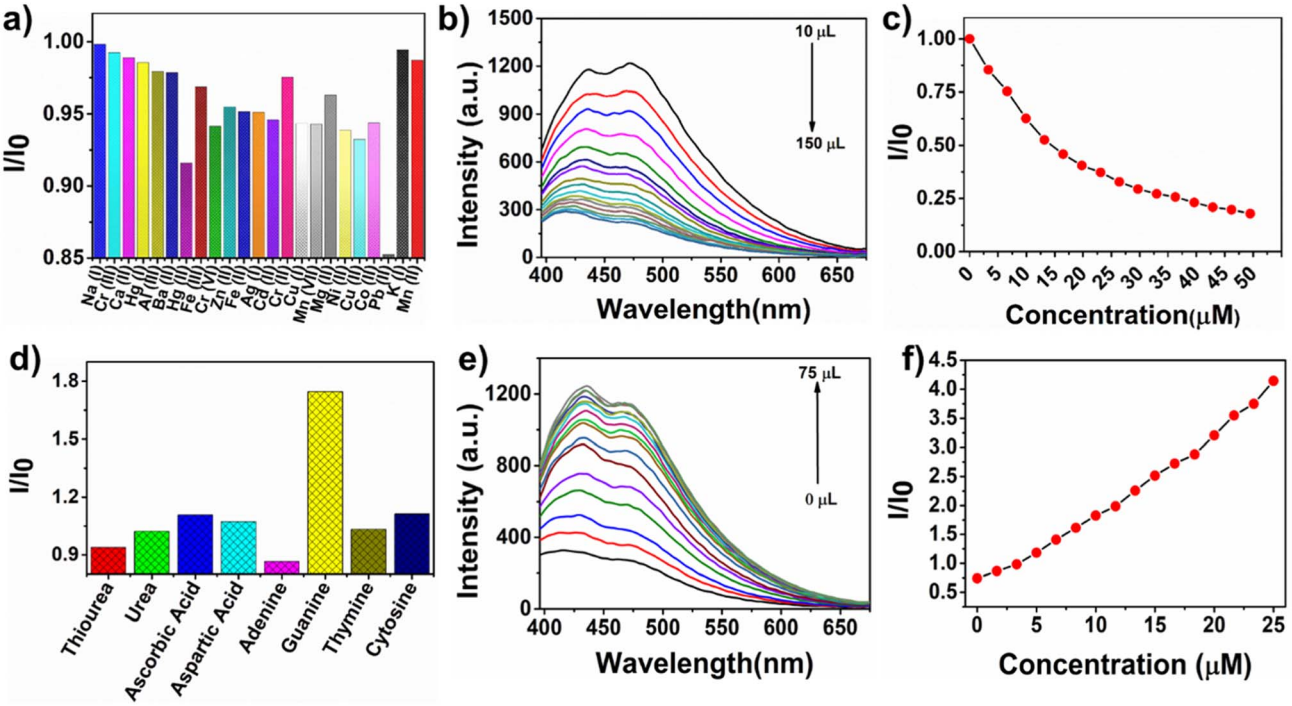


Fig. 4 (a) The selectivity of ws-NGNSs as an optical probe towards $Pb^{2+}$ in the presence of different metal ions. (b) Fluorescence spectra of ws-NGNSs after the incremental addition of $Pb^{2+}$. (c) A plot of the fluorescence intensity ratio *vs.* $Pb^{2+}$ ion concentration. (d) The selective sensing of guanine in the presence of different interfering biomolecules by the ws-NGNSs/$Pb^{2+}$ system. (e) Fluorescence spectra of ws-NGNSs after the incremental addition of guanine. (f) A plot of the fluorescence intensity ratio *vs.* guanine concentration.

contact.[59] This dramatically promoted the charge transfer between ws-NGNSs and $Pb^{2+}$ and resulted in the quenching of the fluorescence intensity of ws-NGNSs. The quenching effect occurred because of the intrinsic emission for electron transfer from the excited state upon the absorption of photons between the fluorophore and selective metal ions.[62] This effect promotes the recombination of electron–hole pairs, followed by a non-radiative process, resulting in fluorescence "turn off".[63] The strong quenching effects of metal ions on the PL emission of ws-NGNSs achieved high sensitivity for the charge transfer mechanism. The lower the energy band gap (the distance between the LUMO and HOMO energy states), the greater the possibility of a non-radiative transition because of the smaller emission gap.[42] The emission gap narrows to a smaller value than the absorption gap during photo-excitation. The surficial functional groups of the ws-NGNSs and the heteroatom doping of the material significantly facilitate the non-radiative transition.[64] When guanine is present in the ws-NGNSs/$Pb^{2+}$ system, it forms a stable complex with $Pb^{2+}$, allowing the surface functional groups of the ws-NGNSs to be free from bonding with $Pb^{2+}$.[65] As a result, the fluorescence intensity is "turned-on". The recovery of fluorescence intensity occurs because of the strong affinity of guanine to bind with $Pb^{2+}$ ions.

# 3. Experimental section

## 3.1 Materials

Rotten pears were collected from the Indian grocery market. Laboratory-grade chemicals were purchased from commercial suppliers and used without any additional purification. All metal ions, except $KMnO_4$, $K_2Cr_2O_7$, and $Al(NO_3)_3 \cdot 9H_2O$ were used as chloride salts and were obtained from Alfa Aesar, India. We procured biomolecules such as glucose, citric acid, dopamine, ascorbic acid, uric acid, adenine, guanine, thymine, and cytosine from Sigma Aldrich, India. All aqueous solutions were prepared with double-distilled water.

## 3.2 Synthesis of ws-NGNSs

The ws-NGNSs were synthesized from rotten pear and urea, which served as the carbon and nitrogen sources, respectively. Crushed rotten pear and urea, in a 6 : 1 ratio, were treated hydrothermally at 220 °C for 48 hours in a Teflon-line coated stainless steel autoclave. The obtained mixture was washed extensively with DI water, to remove water-soluble contaminants, and dried in a hot air oven. After drying, the sample was pyrolyzed in a tube furnace with an inert environment at 600 °C for 2 hours for graphitization. Afterwards, the obtained mixture was treated with 30% nitric acid and excess acid was neutralized with NaOH. The excess NaOH was removed by simply washing with DI water. The obtained mixture was dried and collected for further applications.

## 3.3 Characterization

The surface morphology and structural analysis of the as-synthesized ws-NGNSs were performed using a SEM microscope, JEOL (JSM-7500F, Japan), operating at 20 kV. TEM, high-resolution TEM (HRTEM) imaging was conducted with a FEI

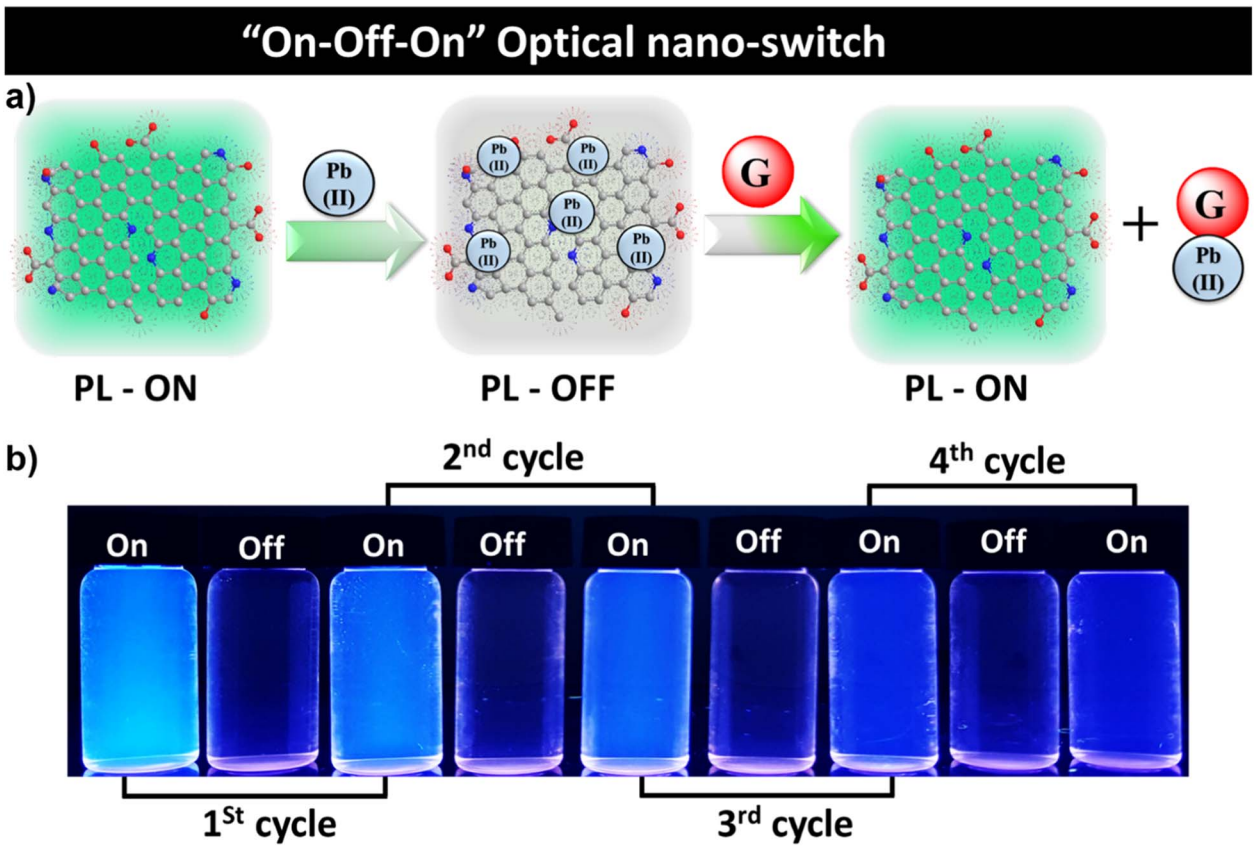


Fig. 5 (a) Schematic representation of the fluorescence "on-off-on" nano-switch for the selective detection of $Pb^{2+}$ and guanine. (b) The digital images demonstrating the cyclic stability of the fluorescence "on-off-on" nano-switch under an irradiation of 365 nm UV light.

Tecnai G2 (Model: F30, USA) electron microscope operating at 300 kV. A Rigaku RINT-2000 (Japan) XRD spectrometer with Cu $K_\alpha$ radiation was used to acquire the XRD patterns of ws-NGNSs in powder form. Raman spectroscopy was conducted using a WITec Raman spectrometer with an Ar laser of 405 nm excitation under ambient temperature. XPS ULVAC-PHI X was used to explore the surface characteristics and bonding environments of the synthesized material. The surface functional groups were examined using a Bruker Vector 22 spectrometer in the 400–4000 $cm^{-1}$ wavenumber range. The UV-vis spectra were obtained at room temperature in aqueous medium using a Varian 50 Bio UV-vis spectrophotometer. A Varian fluorescence spectrometer was used to record the PL properties ws-NGNSs and selectivity measurements.

### 3.4 Sensing experiments

Aqueous solutions of ws-NGNSs 30 μg $mL^{-1}$ were used for all the experiments related to the detection and discrimination of metal ions and biomolecules at room temperature. The fluorescence excitation wavelength was fixed at 340 nm and responses were analyzed by monitoring the changes in PL intensity. The concentration of each metal ion and biomolecule solution used for the study was 1 mM unless otherwise stated. Typically, 10 μL solutions of different metal ions ($Na^+$, $K^+$, $Ag^+$, $Cu^+$, $Cu^{2+}$, $Ni^{2+}$, $Zn^{2+}$, $Hg^+$, $Hg^{2+}$, $Ba^{2+}$ $Ca^{2+}$, $Pb^{2+}$, $Cr^{6+}$, $Cr^{3+}$, $Cr^{2+}$, $Mg^{2+}$, $Mn^{7+}$, $Mn^{2+}$, $Mo^{6+}$, $Fe^{2+}$, $Fe^{3+}$, $Sb^{3+}$, and $Cd^{2+}$) were added to the aqueous solution of ws-NGNSs (2.5 mL), separately and the changes in PL intensity were measured after 10 minutes. In detecting guanine, different guanine concentrations were added to the quenched solution of ws-NGNSs/$Pb^{2+}$ system and the PL intensity was measured after 10 min. Various biomolecules, including adenine, guanine, thymine, cytosine, aspartic acid, ascorbic acid, urea, and thiourea, were added to the ws-NGNSs/$Pb^{2+}$ system under similar experimental conditions to determine the selectivity.

## 4. Conclusion

A fluorescence sensor based on the PL "on-off-on" responses of water-soluble N-doped graphene nanosheets (ws-NGNSs) has been developed. ws-NGNSs were synthesized from rotten pear (carbon source) and urea (nitrogen source) using a facile and green hydrothermal approach followed by mild oxidation. The ws-NGNSs exhibited blue-green emissions with good fluorescence stability, which were used in the development of a simple, rapid, economical and sensitive optical nano-switch for the detection and discrimination of heavy metal ion $Pb^{2+}$ and biomolecule guanine. The addition of $Pb^{2+}$ solution to a ws-NGNSs solution quenched the blue-green emission of ws-NGNSs, which was selectively restored by the addition of guanine. The PL quenching and restoration can also be

detected by the naked eyes under illumination with UV light. Moreover, the "on-off-on" responses are highly reversible and hold significant potential for the fabrication of optical nano-switches.

## Conflicts of interest

The authors declare no conflict of interest.

## Acknowledgements

KMT acknowledges financial assistance from the Department of Biotechnology (DBT), India, through the Ramalingaswami Faculty Award (BT/RLF/Re-entry/45/2018). RKG acknowledges financial assistance from Science and Engineering Research Board, Department of Science & Technology, Government of India (Project No. CRG/2021/007464).

## References

1 P. Yang, W. Bai, Y. Zou, X. Zhang, Y. Yang, G. Duan, J. Wu, Y. Xu and Y. Li, *Mater. Horiz.*, 2023, **10**, 1020–1029.
2 F. Lu and D. Astruc, *Coord. Chem. Rev.*, 2020, **408**, 213180.
3 J. Wang, X. Kong, M. Yang, W. Xiong, Z. Li, H. Zhou, G. I. N. Waterhouse, S.-M. Xu, H. Yan, Y.-F. Song, H. Duan and Y. Zhao, *Ind. Eng. Chem. Res.*, 2023, **62**, 365–374.
4 K. M. Omer and M. Sartin, *Opt. Mater.*, 2019, **94**, 330–336.
5 K. H. Hama Aziz, K. M. Omer and R. F. Hamarawf, *New J. Chem.*, 2019, **43**, 8677–8683.
6 S. H. Al-Jaf and K. M. Omer, *Int. J. Environ. Anal. Chem.*, 2022, 1–14.
7 M. R. Awual, *J. Environ. Chem. Eng.*, 2019, **7**, 103124.
8 H. Zhu, J. Yuan, X. Tan, W. Zhang, M. Fang and X. Wang, *Environ. Sci.: Nano*, 2019, **6**, 261–272.
9 G. Zhou, C. Liu, Y. Tang, S. Luo, Z. Zeng, Y. Liu, R. Xu and L. Chu, *Chem. Eng. J.*, 2015, **280**, 275–282.
10 Z. Khoshbin, M. R. Housaindokht, A. Verdian and M. R. Bozorgmehr, *Biosens. Bioelectron.*, 2018, **116**, 130–147.
11 F. Ahmed, S. Iqbal, L. Zhao and H. Xiong, *Anal. Chim. Acta*, 2021, **1183**, 338977.
12 X. Xu, L. He, Y. Long, S. Pan, H. Liu, J. Yang and X. Hu, *Sens. Actuators, B*, 2019, **279**, 44–52.
13 J. Chen, S. Li, Y. Chen, J. Yang and J. Dong, *Microchim. Acta*, 2022, **189**, 328.
14 L. Yang, T. Zhang, H. Zhou, F. Yan and Y. Liu, *Front. Nutr.*, 2022, **9**, 987442.
15 X. Niu, W. Yang, J. Ren, H. Guo, S. Long, J. Chen and J. Gao, *Electrochim. Acta*, 2012, **80**, 346–353.
16 B. Thomas, S. Matson, V. Chopra, L. Sun, S. Sharma, S. Hersch, H. Diana Rosas, C. Scherzer, R. Ferrante and W. Matson, *Anal. Biochem.*, 2013, **436**, 112–120.
17 F. Tian, X. Jiang, X. Dou, Q. Wu, J. Wang and Y. Song, *Spectrochim. Acta, Part A*, 2017, **179**, 194–200.
18 F. Ahmed, H. Kabir and H. Xiong, *Front. Chem.*, 2020, **8**, 591958.
19 M. Arvand, M. Sanayeei and S. Hemmati, *Biosens. Bioelectron.*, 2018, **102**, 70–79.
20 H. Guo, T. Zhang, M. Wang, L. Sun, J. Zhang, M. Yang, F. Yang, N. Wu and W. Yang, *Colloids Surf., A*, 2021, **627**, 127195.
21 K. Chetankumar, B. E. K. Swamy and H. S. B. Naik, *Mater. Chem. Phys.*, 2021, **267**, 124610.
22 I. J. Bazany-Rodríguez, M. K. Salomón-Flores, J. M. Bautista-Renedo, N. González-Rivas and A. Dorazco-González, *Inorg. Chem.*, 2020, **59**, 7739–7751.
23 N. De Acha, C. Elosúa, J. M. Corres and F. J. Arregui, *Sensors*, 2019, **19**, 599.
24 J. Kaushik, Gunture, K. M. Tripathi, R. Singh and S. K. Sonkar, *Chemosphere*, 2022, **287**, 132105.
25 A. Sharma, N. Sharma, A. Kumari, H.-J. Lee, T. Kim and K. M. Tripathi, *Appl. Mater. Today*, 2020, **18**, 100467.
26 G. S. Das, K. M. Tripathi, G. Kumar, S. Paul, S. Mehara, S. Bhowmik, B. Pakhira, S. Sarkar, M. Roy and T. Kim, *New J. Chem.*, 2019, **43**, 14575–14583.
27 Q. Y. Zhu, F. R. Zhang, Y. Du, X. X. Zhang, J. Y. Lu, Q. F. Yao, W. T. Huang, X. Z. Ding and L. Q. Xia, *ACS Appl. Mater. Interfaces*, 2019, **11**, 8904–8914.
28 P. A. Denis, *ACS Omega*, 2022, **7**, 45935–45961.
29 S. Ullah, Q. Shi, J. Zhou, X. Yang, H. Q. Ta, M. Hasan, N. M. Ahmad, L. Fu, A. Bachmatiuk and M. H. Rümmeli, *Adv. Mater. Interfaces*, 2020, **7**, 2000999.
30 S. Hu, Q. Chang, K. Lin and J. Yang, *Carbon*, 2016, **105**, 484–489.
31 C. Murugesan, B. Senthilkumar and P. Barpanda, *ACS Sustain. Chem. Eng.*, 2022, **10**, 9077–9086.
32 B. Yan, J. Zheng, L. Feng, W. Chen, W. Yang, Y. Dong, S. Jiang, Q. Zhang and S. He, *Diamond Relat. Mater.*, 2022, **128**, 109238.
33 M. Park, A. Sharma, C. Kang, J. Han, K. M. Tripathi and H.-J. Lee, *ACS Biomater. Sci. Eng.*, 2022, **8**, 2131–2141.
34 A. Anouar, A. Grirrane, E. Álvarez, N. Katir, A. Primo, H. Garcia and A. El Kadib, *Mater. Today Sustain.*, 2022, **18**, 100109.
35 N. Dhiman, S. Ghosh, Y. K. Mishra and K. M. Tripathi, *Mater. Adv.*, 2022, **3**, 3101–3122.
36 A. Sharma, R. K. Sharma, Y.-K. Kim, H.-J. Lee and K. M. Tripathi, *J. Environ. Chem. Eng.*, 2021, **9**, 106656.
37 S. Shukla, I. Khan, V. K. Bajpai, H. Lee, T. Kim, A. Upadhyay, Y. S. Huh, Y.-K. Han and K. M. Tripathi, *ACS Appl. Mater. Interfaces*, 2019, **11**, 18165–18177.
38 G. S. Das, A. Bhatnagar, P. Yli-Pirilä, K. M. Tripathi and T. Kim, *Chem. Comm.*, 2020, **56**, 6953–6956.
39 H.-L. Guo, P. Su, X. Kang and S.-K. Ning, *J. Mater. Chem. A*, 2013, **1**, 2248–2255.
40 J. Tian, R. Liu, Z. Liu, C. Yu and M. Liu, *Chin. J. Catal.*, 2017, **38**, 1999–2008.
41 T. Kavitha and S. Kumar, *Sci. Rep.*, 2018, **8**, 16269.
42 T. Anusuya, V. Kumar and V. Kumar, *Chemosphere*, 2021, **282**, 131019.
43 G. S. Das, J. Y. Hwang, J.-H. Jang, K. M. Tripathi and T. Kim, *ACS Appl. Energy Mater.*, 2022, **5**, 6663–6670.
44 Y. Myung, S. Jung, T. T. Tung, K. M. Tripathi and T. Kim, *ACS Sustain. Chem. Eng.*, 2019, **7**, 3772–3782.

45 D. Qu, M. Zheng, P. Du, Y. Zhou, L. Zhang, D. Li, H. Tan, Z. Zhao, Z. Xie and Z. Sun, *Nanoscale*, 2013, **5**, 12272–12277.
46 R. Aggarwal, S. K. Sonkar and K. M. Tripathi, *Carbon*, 2023, **208**, 436–442.
47 K. M. Tripathi, T. S. Tran, Y. J. Kim and T. Kim, *ACS Sustain. Chem. Eng.*, 2017, **5**, 3982–3992.
48 G. S. Das, S. Sarkar, R. Aggarwal, S. K. Sonkar, J.-W. Park, K. M. Tripathi and T. Kim, *Carbon Lett.*, 2019, **29**, 595–603.
49 B. Pakhira, A. Samanta, G. S. Das and S. Sarkar, *ChemistrySelect*, 2017, **2**, 5564–5569.
50 M. A. Zafar, O. K. Varghese, F. C. Robles Hernandez, Y. Liu and M. V. Jacob, *ACS Appl. Mater. Interfaces*, 2022, **14**, 5797–5806.
51 S. Ghosh, S. Barg, S. M. Jeong and K. Ostrikov, *Adv. Energy Mater.*, 2020, **10**, 2001239.
52 L. Qu, Y. Liu, J.-B. Baek and L. Dai, *ACS Nano*, 2010, **4**, 1321–1326.
53 Y. Li, Y. Zhao, H. Cheng, Y. Hu, G. Shi, L. Dai and L. Qu, *J. Am. Chem. Soc.*, 2012, **134**, 15–18.
54 P. Sharma and M. S. Mehata, *Mater. Res. Bull.*, 2020, **131**, 110978.
55 C. Dalal, A. K. Garg, M. Mathur and S. K. Sonkar, *ACS Appl. Nano Mater.*, 2022, **5**, 12699–12710.
56 Y. Feng, N. Jiang, D. Zhu, Z. Su and M. R. Bryce, *J. Mater. Chem. C*, 2020, **8**, 11540–11545.
57 A. Biranje, N. Azmi, A. Tiwari and A. Chaskar, *J. Fluoresc.*, 2021, **31**, 1241–1250.
58 N. B. Brahim, N. B. H. Mohamed, M. Echabaane, M. Haouari, R. B. Chaâbane, M. Negrerie and H. B. Ouada, *Sens. Actuators, B*, 2015, **220**, 1346–1353.
59 H. Sun, N. Gao, L. Wu, J. Ren, W. Wei and X. Qu, *Chem. - Eur. J.*, 2013, **19**, 13362–13368.
60 J. Chen, Y. Gao, C. Guo, G. Wu, Y. Chen and B. Lin, *Spectrochim. Acta, Part A*, 2008, **69**, 572–579.
61 R. Aggarwal, A. K. Garg, V. Kumar, H. Jonwal, S. Sethi, S. Gadiyaram, S. K. Sonkar, A. K. Sonker and G. Westman, *ACS Appl. Nano Mater.*, 2023, **6**, 6518–6527.
62 Y. Liu, W. Q. Loh, A. Ananthanarayanan, C. Yang, P. Chen and C. Xu, *RSC Adv.*, 2014, **4**, 35673–35677.
63 A. L. Koner, P. P. Mishra, S. Jha and A. Datta, *J. Photochem. Photobiol., A*, 2005, **170**, 21–26.
64 S. Chen, N. Ullah, T. Wang and R. Zhang, *J. Mater. Chem. C*, 2018, **6**, 6875–6883.
65 N. De Acha, C. Elosúa, J. M. Corres and F. J. Arregui, *Sensors*, 2019, **19**, 599.